Shock Waves (1999) 9: 87–93

Shock Waves

Massively separated flows due to transverse sonic jet in laminar hypersonic stream

N. Qin[1], A. Redlich[2]

[1] College of Aeronautics, Cranfield University, Cranfield, Beds MK43 0AL, UK
[2] Institute of Aerodynamics and Gasdynamics, University of Stuttgart, Germany

Received 30 June 1998 / Accepted 27 September 1998

Abstract. A numerical simulation of flow interactions due to a transverse sonic jet ejected from a two-dimensional slot into a hypersonic stream is carried out to examine the capability of Navier–Stokes solutions in predicting a massively separated flow upstream of the jet exit. Grid sensitivity has been studied using gradually refined meshes to address the numerical accuracy of the discretised solution of the governing equations. Comparison has been made with published experimental data regarding the separation and reattachment points and the pressure distribution in the separated region. Flow field visualisation provides further insight into the interaction region and reveals a small clockwise vortex immediately ahead of the jet exit, which is found to be responsible for the second peak in the surface pressure distribution.

Key words: Sonic jet, Hypersonic viscous flow, Navier–Stokes solution, Laminar separation

1 Introduction

Transverse jet injection into a supersonic or hypersonic stream has attracted many investigators due to its practical importance in reaction control systems for spacecraft, trust vector control of rocket motors and supersonic combustion of scramjet engines. The interaction of the jet with the external flow results in a complicated flow field involving shock waves, shear layers and large separated regions. Early research in this field has been limited mainly to wind tunnel experiments through Schlieren pictures or shadowgraphs and surface pressure measurements, such as that conducted by Sterrett and Barber (1966). Recently Powrie et al. (1992, 1993) have used liquid crystal thermography (LCT) to visualise the surface heat transfer variation due to jet interaction in addition to surface oil flows in order to locate more precisely the separation and reattachment lines. Development in Navier–Stokes solutions in the recent years has also provided the possibility of numerical simulation of the complicated flow field so that further insight into the interaction problem can be achieved (Shang et al. 1989, Rizzetta 1992, Qin and Foster 1996).

Most of the experimental and computational studies are for turbulent jet interaction problems and corresponding experimental studies employed a variety of turbulence models varying from algebraic models to two equation models. Rizzetta (1992) carried out a numerical study of the slot injection experiments of Aso et al. (1991) and reported improvement of results by using compressibility corrections to a low Reynolds number k-ε model. For numerical simulation of turbulent jet interaction problems, inadequate turbulence modelling has often been held responsible for disagreement between the experiments and the computations. While higher order turbulence modelling is expected to produce better physical modelling, some investigators have recently reported that two-equation models do not offer better results than those of some algebraic models. For example, Clark and Chan (1993) observed no improvement in using the k-ε turbulence model as compared with using the Baldwin-Lomax algebraic model but significant change of results against streamwise grid resolution. Dhinagaran and Bose (1995) compared the algebraic model and the k-ε two-equation model used by Rizzatta for the same flow problem and reached similar conclusion that the higher order model did not perform better and, on the contrary, the algebraic model produced slightly better results downstream of the jet exit.

In view of the controversial aspects in turbulence modelling for this complicated flow problem, it is desirable to investigate the numerical accuracy of the computational simulation of such problems to exclude the influence of the numerical dissipation on the judgement of different turbulence models. To separate the numerical issues from the modelling issues, an ideal validation of the numerical accuracy for jet interaction problem is to find some reliable laminar experimental data.

Powrie et al. (1992, 1993) noticed that there were few experimental data available for laminar hypersonic jet interaction flows, a combination that will be encountered by re-entry and high altitude vehicles over some portion

of the flight path. A series of experimental tests were carried out to study both two-dimensional slot injection and three-dimensional circular jet interaction problems. The laminar jet interaction produces generally a much larger interaction region than that for turbulent cases, which poses a challenge to the accuracy of the numerical simulation in predicting massively separated jet interaction flows.

This paper presents a numerical study of a transverse sonic jet ejected normally into a laminar hypersonic main stream. The flow conditions were chosen to match the experimental work by Powrie et al. (1992, 1993). The separation and reattachment points, the flow interactions in the massively separated region and the surface pressure have been compared with the experimental data. The sensitivity of the solution to different grid densities has been studied to address the numerical accuracy.

2 Methodology

2.1 Governing equations

The governing equations are the two-dimensional compressible Navier–Stokes equations for perfect gas. The law of conservation of mass, momentum and energy over a control volume V bounded by a surface S can be expressed in an integral form as

$$\frac{\partial}{\partial t}\int_V \boldsymbol{Q} dV + \int_S (\boldsymbol{H}\cdot\boldsymbol{n}) dS = 0 \tag{1}$$

which, for steady flows, reduces to

$$\int_S (\boldsymbol{H}\cdot\boldsymbol{n}) dS = 0 \tag{2}$$

The flux tensor $\boldsymbol{H}$ can be written in terms of the Cartesian fluxes as

$$\boldsymbol{H} = \left(\boldsymbol{E}^i - \boldsymbol{E}^v\right)\boldsymbol{i} + \left(\boldsymbol{F}^i - \boldsymbol{F}^v\right)\boldsymbol{j} \tag{3}$$

where $\boldsymbol{i}$ and $\boldsymbol{j}$ are the Cartesian unit vectors and $\boldsymbol{E}^i$, $\boldsymbol{F}^i$ and $\boldsymbol{E}^v$, $\boldsymbol{F}^v$ are the corresponding convective and diffusive Cartesian fluxes respectively. $\boldsymbol{Q}$ in Eq. (1) is the conservative variable vector. They are defined as

$$\boldsymbol{Q} = \begin{pmatrix} \rho \\ \rho u \\ \rho v \\ E_t \end{pmatrix},$$

$$\boldsymbol{E}^i = \begin{pmatrix} \rho u \\ \rho u^2 + p \\ \rho uv \\ (E_t + p)\, u \end{pmatrix}, \quad \boldsymbol{F}^i = \begin{pmatrix} \rho v \\ \rho uv \\ \rho v^2 + p \\ (E_t + p)\, v \end{pmatrix},$$

$$\boldsymbol{E}^v = \begin{pmatrix} 0 \\ \tau_{xx} \\ \tau_{xy} \\ u\tau_{xx} + v\tau_{xy} - q_x \end{pmatrix},$$

$$\boldsymbol{F}^v = \begin{pmatrix} 0 \\ \tau_{xy} \\ \tau_{yy} \\ u\tau_{xy} + v\tau_{yy} - q_y \end{pmatrix},$$

where ρ is the density, u, v the velocity components, p the pressure and E_t the total energy, $\boldsymbol{\tau}$ the stress tensor and $\boldsymbol{q}$ the heat transfer vector related to the temperature gradient.

According to the experiment, the incoming flow boundary layer is laminar before the interaction region under the given flow conditions. However there is no guarantee that the flow shall remain laminar in the interaction region and downstream. Indeed, jet flows are mostly associated with shear layer instability and flow transition. For the present case ahead of the jet exit, no flow unsteadiness was observed in the experiment and a massively separated flow region was identified in the surface flow visualisation. As shown in Aso et al. (1991), turbulent jet interactions tend to produce a much smaller separated region upstream of the jet exit as compared to that induced by a laminar jet interaction. Due to the hugely different behaviour of laminar and turbulent jet interactions, it is reasonable to assume that the flow in front of the jet exit is laminar for the present case.

One important finding from Powrie et al.'s experimental work is the three-dimensionality of the flow downstream of the jet exit after the reattachment region of the downstream vortex. Spanwise quasi-periodic surface pictures were observed in both the surface oil flow and surface heat transfer visualisation after the reattachment line. This highly complicated three-dimensional reattachment process was attributed to the longitudinal vortices due to the Götler instability mechanism operating in the curved separated shear layer. In the present numerical study, no attempt has been made to simulate the three-dimensionality after the interaction region and it is assumed that the interaction is two-dimensional.

The working gas in the present problem is Nitrogen and, therefore, the corresponding gas constants in the above governing equations are $R = 296.8$, $\gamma = 1.4$ and $Pr = 0.72$. The molecular viscosity for Nitrogen is calculated using a polynomial of third order for temperature to fit the Nitrogen data from the table of Vargarftik (1975).

2.2 Finite-volume discretisation

Equations (1) and (2) are expressions of the conservation laws, and are valid for each local discretised finite volume cells as well as for the global control volume. In the present finite volume discretisation, the region of interest is divided into cells denoted by (i, j). Applying the conservation laws (1) to cell (i, j) and assuming that the tensor $\boldsymbol{H}$ remains constant across each face of the cell and that the cell face area vectors are oriented in the positive co-ordinate directions, Eq. (1) may be written as

$$\begin{aligned} &\frac{\partial}{\partial t}\left(V_{i,j}\boldsymbol{Q}_{i,j}\right) \\ &+\boldsymbol{H}_{i+1/2,j}\cdot d\boldsymbol{S}_{i+1/2,j} - \boldsymbol{H}_{i-1/2,j}\cdot d\boldsymbol{S}_{i-1/2,j} \\ &+\boldsymbol{H}_{i,j+1/2}\cdot d\boldsymbol{S}_{i,j+1/2} - \boldsymbol{H}_{i,j-1/2}\cdot d\boldsymbol{S}_{i,j-1/2} = 0 \end{aligned} \tag{4}$$

2.3 Osher's high resolution solver

The numerical integration scheme produces volume-average flow properties, which are assigned to the locations of the cell centres of the cells. An algorithm is to be determined for the evaluation of the flux vectors at the interfaces, which combines two distinct sets of state quantities, representing the states on both side of the interface, into one set of fluxes normal to the interfaces. The conservation laws in (5) can also be written as:

$$\frac{\partial}{\partial t}\left(V_{i,j}\boldsymbol{Q}_{i,j}\right) = -\left(\tilde{\boldsymbol{E}}_{i+1/2,j} - \tilde{\boldsymbol{E}}_{i-1/2,j} + \tilde{\boldsymbol{F}}_{i,j+1/2} - \tilde{\boldsymbol{F}}_{i,j-1/2}\right) \tag{5}$$

To account for the inviscid interaction of the adjacent fluid cells at their interface, a local wave system is solved using the approximate Riemann solver based on Osher's scheme (Osher and Solomon 1982, Osher and Chacravarthy 1983). It leads to the flux formula for the convective term as

$$\tilde{\boldsymbol{E}}^{i}_{i+1/2,j} = \frac{1}{2}\left[\bar{\boldsymbol{E}}^{i}\left(Q^{-}, d\boldsymbol{S}_{i+1/2,j}\right) + \bar{\boldsymbol{E}}^{i}\left(\boldsymbol{Q}^{+}, d\boldsymbol{S}_{i+1/2,j}\right) - \int_{\boldsymbol{Q}^{-}}^{\boldsymbol{Q}^{+}} \left|\frac{\partial \bar{\boldsymbol{E}}^{i}}{\partial \boldsymbol{Q}}\right| d\boldsymbol{Q}\right] \tag{6}$$

where

$$\bar{\boldsymbol{E}}^{i}\left(\boldsymbol{Q}, d\boldsymbol{S}_{i+1/2,j}\right) = \left(\boldsymbol{i}\cdot d\boldsymbol{S}_{i+1/2,j}\right)\boldsymbol{E}^{i} + \left(\boldsymbol{j}\cdot d\boldsymbol{S}_{i+1/2,j}\right)\boldsymbol{F}^{i} \tag{7}$$

The superscript 'i' indicates *inviscid* or *convective* part of the total flux. The integral in (7) is carried out along a path piecewise parallel to the eigenvectors of the Jacobian. The order in which the three eigenvalues are associated with the three subpaths linking the two states $\boldsymbol{Q}^{+}$ and $\boldsymbol{Q}^{-}$ can substantially vary the cost for the approximate Riemann solver. The P-variant ordering has been used in the present evaluation of the integral in (7). In this way only one flux evaluation of (8) is actually required for each of the interface fluxes at most of the cell interfaces (i.e. either subsonic or supersonic points except shock points) while Osher's original ordering of the subpaths in the integral requires three flux evaluations for the subsonic points. In three-dimensional problem, there are three such interface fluxes (even for supersonic flows, two of these could be subsonic) to be calculated for each cell. Thus the saving in computation is significant.

The definition of the states $\boldsymbol{Q}^{-}$ and $\boldsymbol{Q}^{+}$ on either side of the interface determines the order of accuracy of the scheme. If they are chosen as $\boldsymbol{Q}_i$ and $\boldsymbol{Q}_{i+1}$ the numerical scheme for the convective terms will only be first order accurate, which is unsatisfactory for most of the practical applications. The order of the accuracy can be improved by a more accurate interpolation for the states $\boldsymbol{Q}^{-}$ and $\boldsymbol{Q}^{+}$, i.e. the κ-scheme or the MUSCL scheme of van Leer (1979). In the present computation $\kappa = 1/3$ and the accuracy for discretisation of the convective terms is therefore third order. A limiter of van Albata type (van Albata et al. 1982) has been used to avoid oscillations near the discontinuities in the solution.

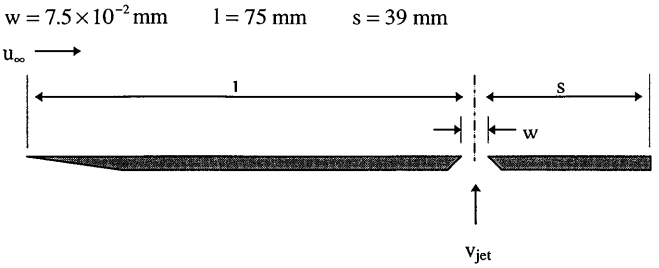

Fig. 1. Slot injection geometry

The calculation of the viscous fluxes is also carried out in a finite-volume manner, where the derivatives of flow properties at the cell interfaces are calculated by creating shifted auxiliary cells and implementing the Green theorem (the Gauss theorem for 3D). In essence, the viscous terms are discretised in a central manner.

The above presented discretisation scheme has been investigated thoroughly by Qin et al. (1991, 1996). It has been found to be capable of capturing both shock waves and shear layers accurately in Navier–Stokes solutions and ideal for Navier–Stokes solutions of complicated flow problems. In such an approach, no artificial viscosity is required in capturing an oscillation-free shock wave.

We are solving steady state problems using a time dependent approach, i.e. we solve (1) to get the solution for (2). As the solution converges, the time dependent term in (6) disappears and a steady state solution is obtained. An explicit multi-stage Runge-Kutta method has been chosen for time integration, which inevitably put an upper limit on the time step used to satisfy the stability condition. For a steady state solution, a local time stepping has been used for a faster convergence of the solution.

3 Results and discussion

3.1 The test case

As mentioned earlier, the computation has been carried out for a test case corresponding to the experimental work in the Southampton University Light Piston Isentropic Compression Tube. The geometric dimension and the jet location are shown in Fig. 1. The incoming flow and the jet conditions are listed in the following two tables.

3.2 Boundary and initial conditions and convergence

The boundary conditions are required at the boundaries of the computational domain for the numerical simulation. At the domain inlet, the incoming hypersonic flow is specified with all the flow properties fixed during the

Table 1. Incoming flow conditions

Free stream gas	Nitrogen
Free stream Mach number M_∞	6.69
Free stream Reynolds number Re_∞/m	4.27×10^6
Free stream total temperature $T_{t\infty}$	628 K
Free stream total pressure $p_{t\infty}$	12.55 bar
Free stream temperature T_∞	63 K
Wall temperature T_w	288 K

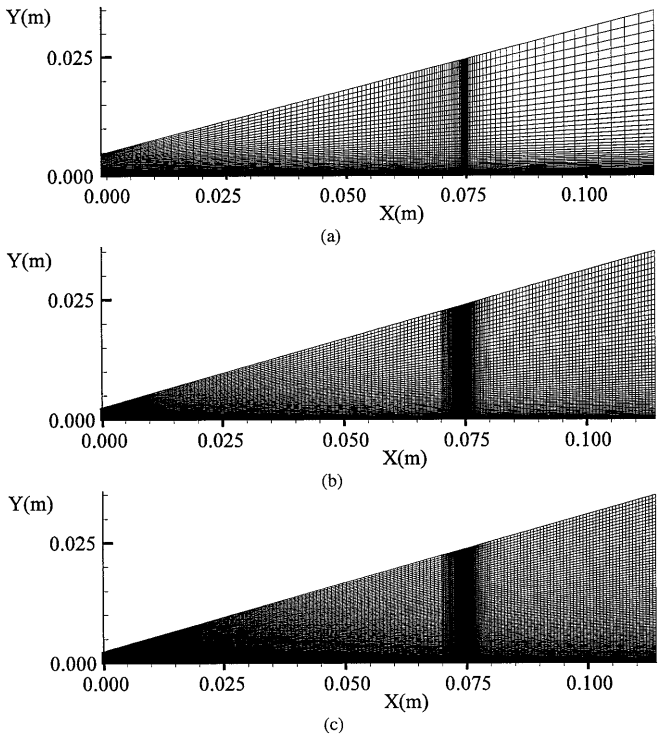

Fig. 2. Computational grids **a** coarse, **b** medium, **c** fine

process of iteration. The top boundary of the domain are treated similarly as the incoming free stream since it is chosen to be outside the leading edge shock wave. At the solid wall, the no-slip boundary condition is implemented, which means both velocity components are set to zero. The other boundary conditions at the wall are: zero pressure gradients normal to the wall and an isothermal temperature boundary condition given in Table 1. At the downstream outlet, all the flow properties are extrapolated from inside the flowfield, as the flow is supersonic outside the boundary layer. Finally at the jet exit, sonic incoming (to the computational domain) flow boundary conditions are specified according to the conditions given in Table 2.

In the time dependent approach, an initial condition of the flowfield is also required to start the iteration process. In the current study, the incoming hypersonic free stream conditions are specified on all the computational cells and the domain boundaries except the solid wall and the jet

Table 2. Jet conditions

Jet gas	Nitrogen
Jet location L	75 mm from leading edge
Jet slot width w	0.075 mm
Jet Mach number M_j	1
Jet total pressure p_{tj}	1.42 bar
Jet total temperature T_{tj}	288 K

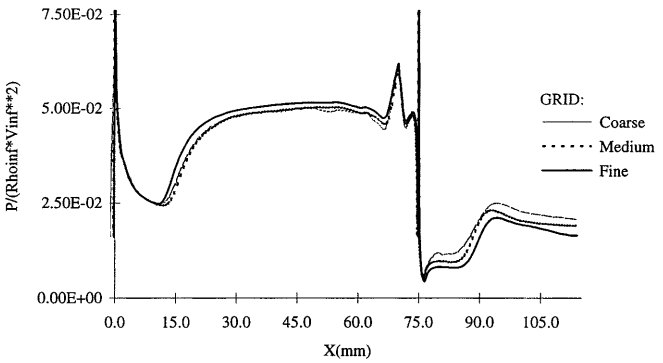

Fig. 3. Grid sensitivity of surface pressure

exit. Convergence of the solution is judged by a reduction of four orders in the residuals defined by the r.m.s. of the right-hand side of (6). All the results presented are converged steady-state solutions by the above criterion.

3.3 Grid sensitivity

For this relatively simple geometry, an algebraic grid generation technique is used, which clusters the grid point towards the wall in the normal direction and towards the jet exit area in the streamwise direction. The outer computational boundary is also inclined for a better resolution of the leading edge region and the leading edge oblique shock wave due to the boundary layer displacement effect. Three different grids, 145×55 (coarse), 301×61 (medium) and 301×101 (fine), as shown in Fig. 2, with progressive refinement, were generated and used in the computation to study the effects of the grid density on the solution.

The flowfield pictures for the three different grids do not give visible differences in the flow features. The coarse grid solution also captures the smallest feature in the problem, the quaternary vortex as discussed later, with the same position and size as the fine grid solution does. For a quantitative comparison, surface pressure distributions from different grid solutions are plotted in Fig. 3, where the results are nondimensional with respect to $\rho_\infty V_\infty^2$. General agreement in the level and trend is observed but slight differences on both sides of the jet are also evident. Without further refining the grid continuously to the point where no change in the solution can be identified (which is a very expensive exercise), the solution on the current fine grid cannot be claimed to be strictly grid-convergent. However the relative low sensitivity of the solution to the

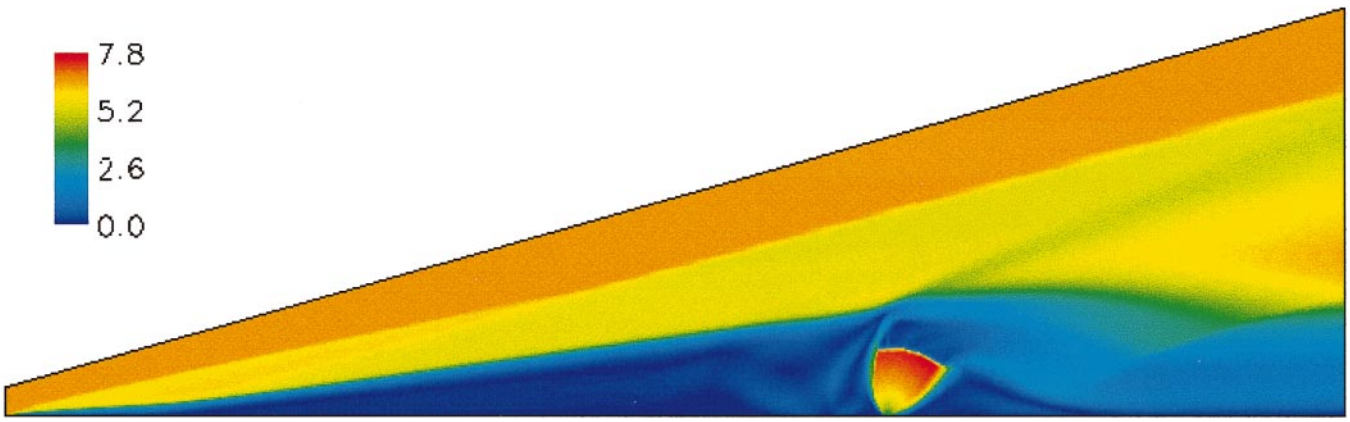

Fig. 4. Mach number contours

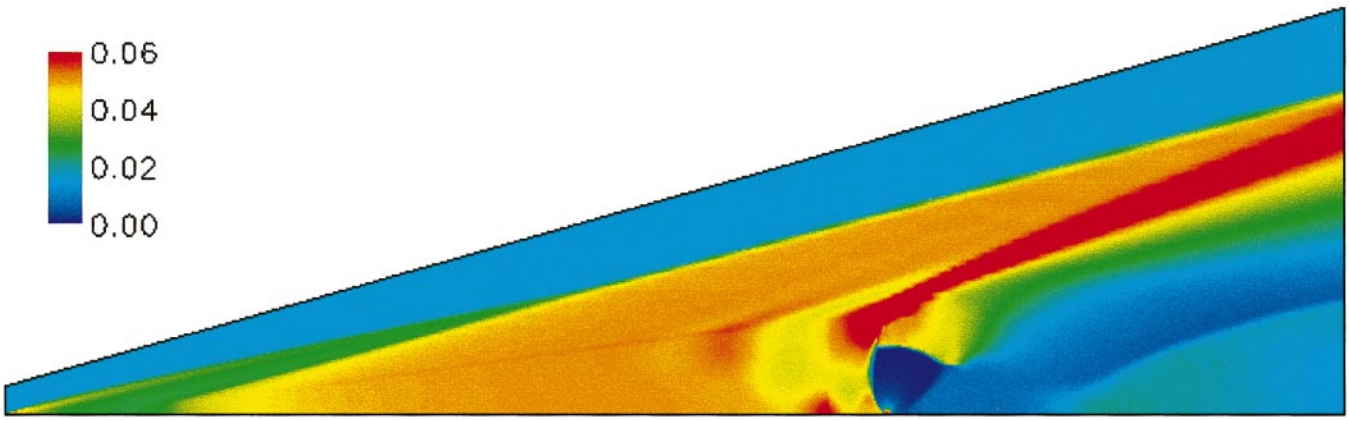

Fig. 5. Pressure contours

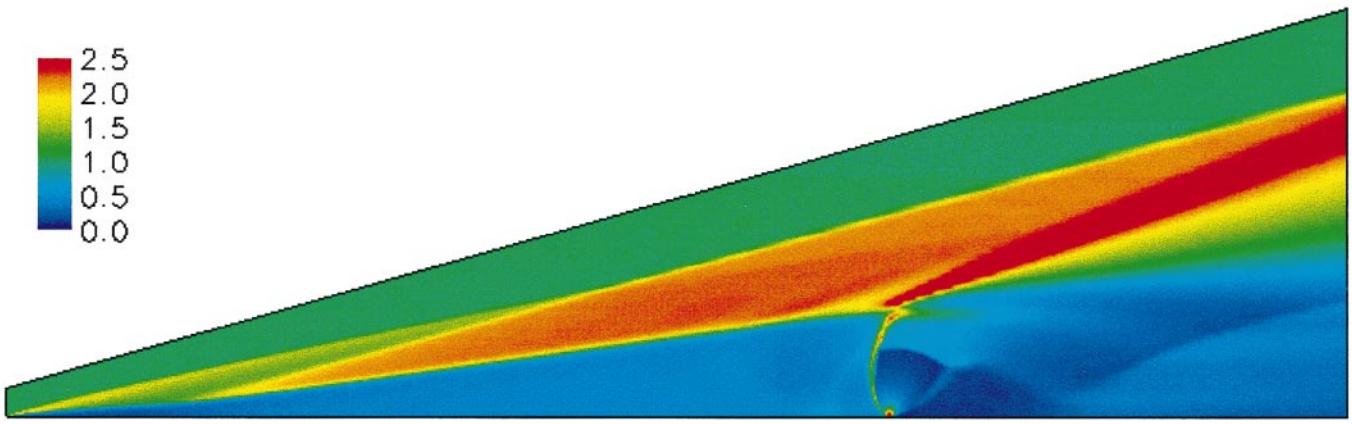

Fig. 6. Density contours

grids indicates that the solution on the grids are reasonably good solutions of the current problem. In the following sections, results on the fine grid will be presented. No further grid refinement was attempted in the current study due to the huge computation involved. For the fine grid, there are 35 grid points inside the boundary layer at the point of primary separation.

3.4 Flow field results and interpretation

The flowfield solution is shown by the Mach number contours in Fig. 4, the pressure contours in Fig. 5, the density contours in Fig. 6 and the streamlines in Fig. 7 with the values indicated in the colour bars. Note that the pressure and density values are nondimensionalised by $\rho_\infty V_\infty^2$ and ρ_∞ respectively in the computation. The boundary layer,

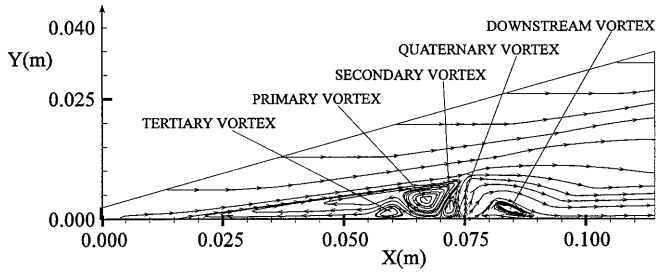

Fig. 7. Streamlines

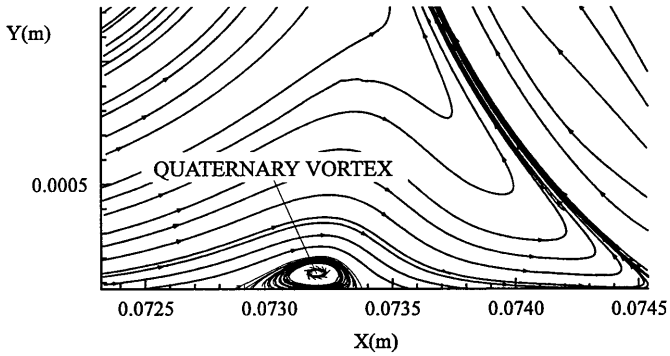

Fig. 8. Enlarged view of the quaternary vortex

the shear layer and the shock wave system are clearly identified in the computed Mach number contours with the help of the pressure and the density contours. The leading edge shock and the separation shock can be observed, which meet each other and combine into a stronger oblique shock wave downstream. In the jet region, a very strong normal shock can be seen, which is known as the 'Mach disc'. The jet boundary and the barrel shaped internal shocks can also be observed on both sides of the jet exit. Above the jet interaction region, an interaction shock can be seen. There is also a recompression shock after the jet interaction region, which turns the downward supersonic flow back parallel to the wall. The incoming boundary layer separates at about 60 mm upstream of the jet exit and an extensive separated region forms. Multiple vortices are developed in this region including a primary vortex and a secondary counter-rotating vortex just upstream of the jet stream. The reverse flow under the primary vortex experiences an adverse pressure gradient and separated to form a tertiary vortex under the primary one. In a magnified picture of the stream lines near the jet exit, Fig. 8, a relatively much smaller quaternary vortex can be observed which is responsible for the significant second peak in the surface pressure distribution near the jet exit.

All the main features ahead of the jet exit are in good agreement with those discussed in the experimental work. However the tertiary vortical flow under the primary vortex was not observed in the experimental surface visualisation. A possible reason is that this vortical flow is driven by the reverse flow and carries little energy so that it leaves too little trace on the surface for the surface visualisation techniques used in the experiment to detect. On the other

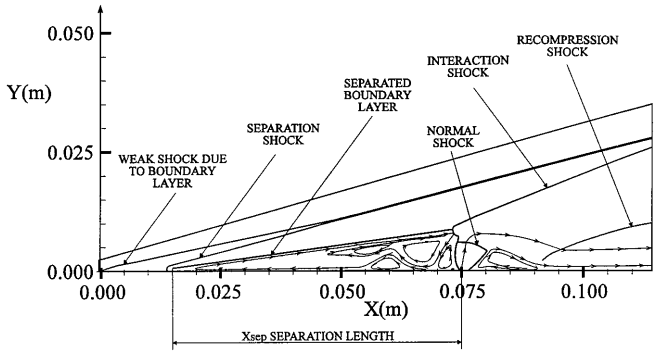

Fig. 9. Schematic of the 2-D Jet interaction flow field

hand, the quaternary vortex, though much smaller, leaves its trace on the surface pressure distribution, as shown in Fig. 8, and its reattachment point corresponds to the secondary peak near the jet exit. This secondary pressure peak has been observed in many other experimental investigations for both laminar and turbulent jet interactions including those reported by Sterret and Barber (1966).

The flowfield features are summarised in Fig. 9, where the flow feature lines are extracted from the contour lines and streamlines in Figs. 4–7. It is clear that the jet interaction has made the flowfield an extremely complicated one involving multiple shocks and vortices. As mentioned earlier, no attempt has been made to simulate the downstream three-dimensionality in the present test and comparisons in the following sections are made only in the interaction region where some quantitative data are available.

3.5 Comparison of primary separation and reattachment points

The primary separation point determines the separation region while the primary reattachment pinpoints the high pressure and high heat transfer region. The separation length was given in the experimental work determined by oil flows and the liquid crystal thermography technique for surface visualisation. The given experimental separation length is 58.6 mm upstream of the jet exit, while the computational separation length is predicted at 60 mm defined by the zero skin friction point. The difference is about 2%, which indicates a very good agreement considering the uncertainties in the experimental measurements. Both computation and experiment give a primary reattachment point at around 5 mm upstream of the jet exit.

3.6 Surface pressure comparison

The surface pressure comparison is made between the experimental measurements and the computation in Fig. 10. The experimental data were normalised by the undisturbed surface pressure distribution on the flat plate. Therefore the computational data were processed accordingly, which

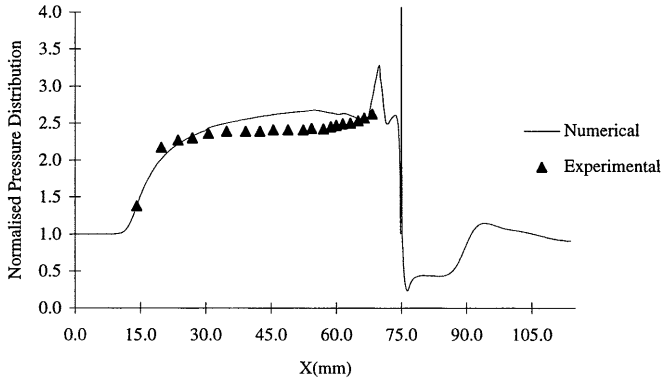

Fig. 10. Comparison of normalised surface pressure

required a separate calculation of the flat plate flow without jet injection. The pressure rise positions are in very good agreement, which is not surprising as the boundary layer separation points are in good agreement. The levels of the pressure plateau in the separated region also compare reasonably well. However the computed surface pressure plateau tends to be slightly higher than the experimental data over a large part of the interaction region. The experimental data exhibit a smoother distribution while the computation predicts a valley before the peak at the reattachment point. There is no experimental data at the reattachment point and downstream to be compared with. The computation also predicts a second peak due to the small vortex near the jet exit. As mentioned before, the second pressure peak is identified as a result of the reattachment of the quaternary vortex immediately upstream of the jet exit.

4 Conclusions

A detailed two-dimensional numerical simulation of a complicated jet interaction in laminar hypersonic flow is presented. The high-resolution of the computed flow filed are primarily due to the high-resolution discretisation scheme, which resolves both shock waves and shear layers accurately. This results in a relatively low grid sensitivity of the solution. The computed separation and reattachment points ahead of the jet exit are in good agreement with the experimental data so that the size of the massively separated interaction region is well predicted. This agreement upstream of the jet exit leads to the conclusion that the interaction is dominated by laminar flows. The numerical simulation provided further insight into the flowfield and associated flow features. The tertiary and quaternary vortices were observed in the simulated flowfield, which are possibly either too weak or too small for the flow visualisation techniques to detect.

It will be interesting to simulate the downstream three-dimensionality in the future for the two-dimensional slot jet. Then a full three-dimensional Reynolds-averaged Navier–Stokes solution will be required with a proper turbulence model and, probably more difficultly, a proper transition model as the flow is certainly laminar in a large part of the interaction region.

Acknowledgements. The authors would like to thank John Edwards of DERA for suggesting the work and Graham Ball of Southampton University for providing the experimental data. The second author also likes to acknowledge the support from the ERASMUS student exchange programme.

References

Aso S, Okujama S, Kawai M (1991) Experimental study of mixing phenomena in supersonic flows with slot injection. AIAA Paper-91-0016

Clark SW, Chan SC (1993) Effects of turbulence models and adaptive grids on the jet interaction flowfield. AIAA Paper 93-3524

Dhinagaran R, Bose TK (1995) Two-dimensional jet interaction flowfiled predictions with an algebraic turbulence model. AIAA Paper 95-2242

Osher S, Solomon F (1982) Upwind difference schemes for hyperbolic systems of conservation laws. Mathematics of Computation, 38(158): 339

Powrie HEG, Ball GJ, East RA (1992) Experimental study of a two dimensional control jet with a hypersonic flow. IUTAM Conference on Aerothermochemistry of Spacecraft and Associated Hypersonic Flows, Marseille, France

Powrie HEG, Ball GJ, East RA (1993) Comparison of the interactions of two and three dimensional transverse jets with a hypersonic free stream. Computational and Experimental Assessment of Jets in Cross Flow. Winchester, UK, AGARD CP-534, Paper 20

Qin N, Foster GW (1996) Computational study of supersonic lateral jet flow interactions. Journal of Spacecraft and Rockets, 33(5): 651

Qin N, Scriba KW, Richards BE (1991) Shock-shock, shock-vortex interection and aerodynamic heating in hypersonic corner flow. Aeronautical J. 95(945): 152

Rizzetta DP (1992) Numerical simulation of slot injection into a turbulent supersonic stream. AIAA J. 30(10): 2434

Shang JS, McMaster DL, Scaggs N, Buck M (1989) Interaction of jet in hypersonic cross stream. AIAA J. 27(3): 323

Sterrett JR, Barber JB (1966) A theoretical and experimental investigation of secondary jets in a Mach 6 free stream with emphasis on the structure of the jet and separation ahead of the jet. Separated Flows Part 2, AGARD-CP-4, pp 667–700

Van Albada GD, van Leer B, Roberts WW (1982) A comparative study of computational methods in cosmic gas dynamics. Astronomy and Astrophysics, 108: 76

Vargaftik NB (1975) Tables on the Thermophysical Properties of Liquids and Gases. Second Edition, John Wiley and Sons

Van Leer B (1979) Towards the ultimate conservative difference scheme V: A second order sequel to Godunov's method. J. Comp. Physics 32: 101